Double-photoionization calculations of the helium metastable $2\,^{1,3}S$ states

A. S. Kheifets, A. Ipatov,* and M. Arifin
Research School of Physical Sciences and Engineering, Australian National University Canberra ACT 0200, Australia

Igor Bray
Electronic Structure of Materials Centre, The Flinders University of South Australia, GPO Box 2100, Adelaide 5001, Australia

(Received 27 June 2000; published 19 October 2000)

Theoretical results are presented for double photoionization and ionization with excitation of the metastable $2\,^{1,3}S$ states of helium. We employ the momentum space formulation of the close-coupling theory to describe nonperturbatively the electron-electron interaction in the final state. A large Laguerre basis is used to obtain convergent close-coupling (CCC) results. In addition, we employ a *B*-spline basis for the target states. The presented results cover continuously the photon energy range from the double-photoionization threshold to the asymptotic limit of infinite photon energy. Near the threshold our data generally support the calculations of van der Hart *et al.* [Phys. Rev. A **57**, 3641 (1998)]. At large photon energies our results merge continuously with the asymptotic values derived from the metastable state $2\,^{1,3}S$ wave functions. Proportionality between the double-to-single photoionization cross-sections ratio and the cross section of electron-impact ionization of the ion is tested to examine the relative contributions of different mechanisms of the two-electron photoionization in the ground and metastable states of the helium atom.

PACS number(s): 32.80.Fb, 34.80.−i

I. INTRODUCTION

A two-electron transition in an atom following absorption of a single photon is a process which is only possible due to electron-electron correlations. Such transitions include excitation photoionization (EPI), where the residual ion is left in an excited state, and double photoionization (DPI). Because of the pivotal role of the electron-electron correlations, the EPI and DPI processes continue to receive considerable attention, both theoretically and experimentally.

The helium atom is the simplest atomic target in which two-electron transitions take place in their purest form. Because of the relative simplicity of the underlying physics much of the experimental and theoretical work involving two-electron ionization has been focused on helium. As a result, a vast amount of experimental and theoretical data are now available on the EPI and DPI from the helium atom. Consistent results are available for the total cross sections as well as the multiply differential cross sections which describe the energy sharing and the angular correlation between the two photoelectrons, see the review of Briggs and Schmidt [1].

The vast majority of studies are limited to the helium atom in its ground state. Comparatively little is known about the two-electron processes in the metastable $2\,^{1,3}S$ states of helium. Although these states are quite stable, particularly the triplet, lack of intense continuous gas sources precludes any experimental studies beyond the simplest one-electron photoionization [2]. This situation may be changing for the better soon with the advent of bright sources of metastable helium utilizing the novel laser cooling and magnetic trapping techniques [3]. In anticipation of the new experiments we feel it is appropriate to revisit the theory of two-electron photoionization from the metastable helium and to bring it to the level which is now achieved for the ground state. Apart from comparison with experiment, a theoretical study of two-electron photoionization from the metastable helium allows extraction of the underlying physics of interest. The three helium states, the ground ^1S and the two metastable $2\,^{1,3}S$, form a sequence in which the relative contributions of different mechanisms of two-electron photoionization are gradually changing. This invites a systematic study by observing the proportionality between the double-to-single photoionization cross-sections ratio and the cross section of the electron impact ionization of the helium ion.

The first theoretical results on the two-electron photoionization from the metastable helium were reported by Norcross [4], Jacobs and Burke [5], and Jacobs [6]. They calculated the EPI to the lowest $n=2$ and $n=3$ ion states. Later these results were superseded by the far more sophisticated calculations of Zhou and Lin [7] who employed the hyperspherical close-coupling method. In a similar study Chang and Zhen [8] used a configuration-interaction procedure for the continuum based on a finite L^2-basis set constructed from a nearly complete set of one-particle hydrogenic orbitals.

The first calculation of the DPI from the metastable helium was reported by Teng and Shakeshaft [9]. The calculation was based on using a final-state wave function which was a product of three Coulomb wave functions modified by a short-range correction term. By investigating the angular distribution in the two-electron continuum the authors were able to estimate the relative contribution of different DPI mechanisms. Forrey *et al.* [10] concentrated their theoretical effort in the asymptotic region of the very high (asymptotically infinite, but still nonrelativistic) photon energies. In this region the many-electron correlation in the final state can be neglected and the whole yield of the singly ionized and ex-

*Permanent address: Department of Experimental Physics, St. Petersburg Technical University, 195251 St. Petersburg, Russia.

cited or doubly ionized states can be calculated from the initial state wave function.

The most complete calculation of the two-electron photoionization from the metastable helium was reported by van der Hart *et al.* [11]. By using the *R*-matrix method they calculated the EPI and DPI cross sections from the threshold to 80 eV excess energy. It is essential for the *R*-matrix method to place the scattering system in a box of a finite size. This produces an unphysical oscillatory structure in the calculated DPI cross section. By averaging over the size of the box the magnitude of the oscillation was significantly reduced, however, they remain clearly visible in the calculation of van der Hart *et al.* [11]. They also noted that the size of the box affected the gauge invariance of their calculation, particularly the length form results.

In the present paper we intend to study the two-electron photoionization from the metastable helium by employing the momentum-space formulation of the close-coupling theory. Based on a large Laguerre basis this theoretical scheme is known in the literature as the convergent close-coupling (CCC) method. Application of the CCC method to the two-electron photoionization in the ground-state helium was very successful. It allowed to produce the accurate total EPI and DPI rates [12–14], to describe the angular correlation in the two-electron continuum [15] and the circular dichroism in the DPI process [16]. Following the same theoretical scheme we hope to produce results of comparable accuracy for the metastable helium. In addition, we use a different implementation of the momentum-space close-coupling theory based on a *B*-spline pseudostate basis. The *B* splines are a flexible and convenient tool which is widely used in theoretical atomic physics [17]. In the present paper we demonstrate that the *B* splines can be successfully used to describe the EPI and DPI processes from the helium ground and metastable states. In the future we hope to utilize the universality of the *B*-spline technique and to extend the close-coupling theory of the two-electron photoionization to more complex atomic targets.

In Sec. II we describe the multiconfiguration Hartree-Fock calculation of the metastable $2\,^{1,3}S$ helium wave functions. In Sec. III we give a brief outline of the CCC theory and the momentum-space formulation of the close-coupling theory using *B* splines. In Sec. IV we present the bulk of our results for the EPI and DPI cross sections from the singlet and triplet metastable helium states. In Sec. V a parallel is drawn between two-electron photoionization and electron-impact ionization of the helium ion. We conclude by summarizing our results in Sec. VI.

II. INITIAL-STATE WAVE FUNCTIONS

In our earlier work on two-electron photoionization from the helium ground state [13] we demonstrated that a highly correlated ground-state wave function was needed to obtain essentially gauge invariant photoionization cross sections. We employed two different types of the ground-state wave functions—the multiconfiguration Hartree-Fock (MCHF) and the explicitly correlated Hylleraas expansion. Both types were found suitable provided sufficient number of configurations are included.

The metastable $2\,^{1,3}S$ helium states are less correlated than the ground ^1S state because the two electrons are well separated in both space and energy. Therefore we have chosen the slightly less accurate, but much more convenient, MCHF wave functions rather than the formidable Hylleraas expansions. The MCHF metastable state wave function is written as an expansion over the two-electron configurations

$$\begin{aligned}\langle \boldsymbol{r}_1\boldsymbol{r}_2|\,2\,^{1,3}S\rangle = \sum_{nl,\,n'l} A_{nl,n'l} N_{nn'} \sum_m C^{00}_{lm,\,l-m} \\ \times[\phi_{nlm}(\boldsymbol{r}_1)\phi_{n'l-m}(\boldsymbol{r}_2) \\ +(-1)^{S_0}\phi_{nlm}(\boldsymbol{r}_2)\phi_{n'l-m}(\boldsymbol{r}_1)]. \qquad (1)\end{aligned}$$

Here the normalization factor $N_{nn'}=1/2$ for $n=n'$ and $1/\sqrt{2}$ for $n\neq n'$. The total spin $S_0=0,1$ for the singlet and triplet states, respectively. The configuration interaction coefficients are normalized to unity: $\Sigma_{nl,\,n'l}A^2_{nl,n'l}=1$. The angular momentum coupling is taken care of by the Clebsch-Gordan coefficients $C^{00}_{lm,\,l-m}$.

The one-electron orbitals in expansion (1) have the form $\phi_{nlm}(\boldsymbol{r})=r^{-1}P_{nl}(r)Y_{lm}(\hat{\boldsymbol{r}})$, where P_{nl} are the radial orbitals and Y_{lm} are the spherical harmonics. The former are found by using the MCHF computer code [18]. First, the single $1s2s$ configuration is calculated. Then the $1s$ and $2s$ orbitals are frozen and subsequently single-electron orbitals nl are added until we are satisfied with the accuracy in terms of the energy and, more importantly, the asymptotic EPI and DPI ratios. As was shown by Dalgarno and Stewart [19] these ratios can be calculated solely from the metastable state wave function through the overlap integrals

$$C_n\propto|\langle ns^+|\,\delta(\boldsymbol{r}_2)|2\,^{1,3}S\rangle|^2, \quad C\propto|\langle 2\,^{1,3}S|\,\delta(\boldsymbol{r}_2)|2\,^{1,3}S\rangle|^2. \qquad (2)$$

In the above expression $\langle ns^+|$ is the one-electron ns orbital of the He^+ ion.

The asymptotic DPI and EPI ratios are then given by

$$R^\infty_n=\left.\frac{\sigma_n}{\sigma^+ +\sigma^{++}}\right|_{\omega\to\infty}=\frac{C_n}{C}, \quad R^\infty=\left.\frac{\sigma^{++}}{\sigma^+}\right|_{\omega\to\infty}=\frac{C-\sum_n C_n}{\sum_n C_n}, \qquad (3)$$

where σ_n is the partial EPI cross section, and $\sigma^+=\Sigma^\infty_{n=1}\sigma_n$ and σ^{++} are the total single- and double-photoionization cross sections. Here we follow notations of Refs. [10,11] and define R_n as the ratio of the partial to the *total* cross sections whereas R is defined as the ratio of the double to *single* cross sections.

Results for R^∞_n and R^∞ are shown in Table I in comparison with the Hylleraas-based calculation of Forrey *et al.* [10]. We see that the MCHF expansions are rapidly convergent and a moderate number of terms is sufficient to approach the Hylleraas results. As compared to the analogous expansions

TABLE I. The binding energy E and the asymptotic ratios R_n^∞ and R^∞ for the helium $2\,^{1,3}S$ metastable states. The MCHF expansions contains 6, 10, and 14 configurations for the singlet state, and 4 and 10 configurations for the triplet state. Configurations included in these expansions are indicated in the table.

	Singlet $2\,^1S$				Triplet $2\,^3S$		
	MCHF6 $1s^2,1s2s,1s3s$ $2s^2,2s3s,2p^2$	MCHF10 $nsn's,n=1\ldots3$ $2p^2,2p3p,3p^2,3d^2$	MCHF14 $nsn's,n=1\ldots4$ $2p^2,2p3p,3p^2,3d^2$	Hylleraas Forrey *et al.* Ref. [10]	MCHF4 $1s2s,1s3s$ $2s3s,2p3p$	MCHF10 $nln'l,n=1\ldots4$ $l=0,1,2$	Hylleraas Forrey *et al.* Ref. [10]
E (eV)	58.333	58.367	58.384	58.395	59.192	59.192	59.191
R_n^∞ $n=1$	0.0479	0.0481	0.0490	0.0493	0.0333	0.0334	0.0338
2	0.5308	0.5352	0.5302	0.5346	0.7777	0.7800	0.7824
3	0.4086	0.4039	0.4040	0.3993	0.1782	0.1761	0.1733
4	0.0027	0.0028	0.0035	0.0035	0.0044	0.0043	0.0044
5	0.0014	0.0014	0.0017	0.0017	0.0014	0.0013	0.0014
6	0.0007	0.0007	0.0009	0.0009	0.0006	0.0006	0.0006
7	0.0004	0.0004	0.0005	0.0005	0.0003	0.0003	0.0003
R^∞ (%)	0.6561	0.6529	0.9206	0.9033	0.3281	0.3138	0.3118

for the ground state helium [13] fewer terms with smaller orbital momenta are needed to achieve comparable accuracy. This indicates a weaker ground state correlation in the metastable states as might be expected. This correlation is the weakest in the triplet metastable state from which the diagonal terms are removed due to the Pauli exclusion principle.

It is to be noted that the ionization-excitation to the $n=2$ and $n=3$ ion states are more probable than to the ground $n=1$ state. This is in a sharp contrast to the ground state EPI where the $n=1$ state is clearly dominant. We shall note this when making a comparison between the two-electron photoionization and electron-impact ionization.

III. FINAL-STATE WAVE FUNCTIONS

A. CCC formalism

A multichannel expansion is used for the final-state wave function of the two-electron system with boundary conditions corresponding to an outgoing wave in a given channel and incoming waves in all other channels. The channel wave function $\langle \boldsymbol{k}^{(-)} n|$ is the product of a one-electron He^+ target orbital Φ_n^N and a (distorted) Coulomb outgoing wave $\chi_{\boldsymbol{k}}^{(-)}$. The target states are obtained by diagonalizing the He^+ Hamiltonian

$$\langle \Phi_n^N|H|\Phi_m^N\rangle=\epsilon_n^N\delta_{nm}, \tag{4}$$

where $H=-\nabla^2/2+Z/r$ and $Z=2$. We write

$$\Phi_n^N(\boldsymbol{r})\equiv\Phi_{nlm}^N(\boldsymbol{r})=r^{-1}P_{nl}^N(r)Y_{lm}(\hat{\boldsymbol{r}}),$$
$$\text{where}\quad P_{nl}^N(r)=\sum_{k=1}^{N} C_{nk}^l\xi_{kl}(r). \tag{5}$$

Here ξ_{kl} are Laguerre polynomials and the coefficients C_{nk}^l are obtained after the diagonalization.

The distorted Coulomb waves satisfy the Schrödinger equation

$$(-\nabla^2/2+U(r)-\varepsilon_k)\chi_{\boldsymbol{k}}^{\pm}=0, \tag{6}$$

where $\varepsilon_k=k^2/2$. The potential $U(r)=(Z-1)/r+U_d(r)$, where $Z-1$ is the asymptotic charge seen by the projectile at large distances. The arbitrary distorting potential satisfies $U_d(r)\to0$ as $r\to\infty$, and is used to reduce the numerical complexity of solving the coupled equations [20]. The Coulomb waves are expanded as

$$\chi_{\boldsymbol{k}}^{\pm}(\boldsymbol{r})=(2/\pi)^{1/2}(kr)^{-1}\sum_{LM} i^L e^{\pm i\delta_L}u_L(k,r)Y_{LM}(\hat{\boldsymbol{r}})Y_{LM}^*(\hat{\boldsymbol{k}}), \tag{7}$$

where σ_L is the phase shift, $u_L(k,r)$ is real and has the asymptotic form

$$u_L(k,r)\to r^{-1}\sin(kr+L\pi/2+\delta_L). \tag{8}$$

The dipole matrix element of the photon induced transition to a given channel can be written as

$$\langle \boldsymbol{k}^{(-)}i|\mathcal{D}|2\,^{1,3}S\rangle=\langle \boldsymbol{k}^{(-)}i|d|2\,^{1,3}S\rangle+\sum_j \sum\!\!\!\!\!\!\int d^3k \times\frac{\langle \boldsymbol{k}^{(-)}i|T_{S_0=0,1}|j\boldsymbol{k}'^{(+)}\rangle\langle \boldsymbol{k}'^{(+)}j|d|2\,^{1,3}S\rangle}{E-k'^2/2-\epsilon_j+i0}. \tag{9}$$

Here $E=k^2/2+\epsilon_i$ is the final-state energy. The first term on the right-hand side of Eq. (9) corresponds to the direct photoionization. The second term describes the two-stage process in which photoionization is followed by scattering of the photoelectron on the residual ion. It contains the half-off-shell dipole T matrix in the singlet ($S_0=0$) or triplet ($S_0=1$) channel which can be found by solving a set of coupled Lippmann-Schwinger integral equations [20].

The dipole electro-magnetic operator d can be written in one of the following forms commonly known as length (L), velocity (V), and acceleration (A) [21]:

$$d^r=\omega(z_1+z_2),$$

$$d^\nabla=\nabla_{z_1}+\nabla_{z_2}, \tag{10}$$

$$d^{\dot\nabla}=\frac{Z}{\omega}\left(\frac{z_1}{r_1^3}+\frac{z_2}{r_2^3}\right),$$

with the z axis chosen along the polarization vector of the photon. We separate the angular dependence of the dipole matrix elements by using the Wigner-Eckart theorem:

$$\langle \boldsymbol{k}^{(-)}i|d|2\ ^{1,3}S\rangle=\frac{1}{\sqrt{3}}\sum_{LM} C^{10}_{l_im_i,\,LM}Y_{LM}(\hat{\boldsymbol{k}}) \times\langle Lk^{(-)}l_in_i\|d\|2\ ^{1,3}S\rangle. \tag{11}$$

Here the reduced dipole matrix element, in the length form, is

$$\langle Lk^{(-)}l_in_i\|d\|2\ ^{1,3}S\rangle=i^{-L}e^{i\delta_L(k)}l_>\sum_{nl,n'l} A_{nl,n'l}N_{nn'}C^{00}_{l0,l0} \times\{\langle Lk\|ln\rangle\langle l_in_i\|r\|ln'\rangle\delta_{lL}+\langle l_in_i\|ln\rangle \times\langle Lk\|r\|ln'\rangle\delta_{l_il}\}, \tag{12}$$

where $l_>=\max(L,l_i)$. In the above expression we introduced the overlap integrals

$$\langle Lk\|ln\rangle=\int_0^\infty dru_L(k,r)P_{nl}(r),$$

$$\langle l_in_i\|ln\rangle=\int_0^\infty drP^N_{n_il_i}(r)P_{nl}(r)$$

and the dipole radial integrals (in the length form)

$$\langle Lk\|r\|ln\rangle=\int_0^\infty rdru_L(k,r)P_{nl}(r),$$

$$\langle l_in_i\|r\|ln\rangle=\int_0^\infty rdrP^N_{n_il_i}(r)P_{nl}(r).$$

The velocity and acceleration forms are given by expressions similar to Eq. (12) in which the dipole radial integrals $\langle\|r\|\rangle$ are substituted by the $\langle\|\partial/\partial r\|\rangle$ and $\langle\|2/r^2\|\rangle$ integrals, respectively.

Following Bray and Stelbovics [22] we strip the angular dependence from the T matrix

$$\langle \boldsymbol{k}^{(-)}i|T_S|j\boldsymbol{k}'^{(+)}\rangle = \sum_{\substack{L,L',J\\ M,M',M_J}} C^{JM_J}_{LM,\,l_im_i}C^{JM_J}_{L'M',\,l_jm_j}Y_{LM}(\hat{\boldsymbol{k}})Y^*_{L'M'}(\hat{\boldsymbol{k}}') \times\langle Lk^{(-)}l_in_i||T_{JS}||n_jl_jk'^{(+)}L'\rangle, \tag{13}$$

and write Eq. (9) in a one-dimensional form

$$\langle Lk^{(-)}n_il_i\|\mathcal{D}\|2\ ^{1,3}S\rangle =\langle Lk^{(-)}n_il_i\|d\|2\ ^{1,3}S\rangle +\sum_{l_jn_j}\sum_L\oint_{k'}\frac{\langle Lk^{(-)}l_in_i||T_{JS_0}||n_jl_j\,k'^{(+)}L'\rangle}{E-k'^2/2-\epsilon_j+i0} \times\langle L'k'^{(+)}l_jn_j\|d\|2\ ^{1,3}S\rangle. \tag{14}$$

Here $J=1$ and $S_0=0,1$ are the total orbital momentum and spin of the electron pair.

The photoionization cross section, as a function of the photon energy ω, corresponding to a particular bound electron state i is given by [21]

$$\sigma_i(\omega)=\frac{4\pi^2}{\omega c}\sum_{m_i}\int d^3k\,|\langle \boldsymbol{k}^{(-)}i|\mathcal{D}|2\ ^{1,3}S\rangle|^2\delta(\omega-E+E_0) =\frac{4\pi^2k}{3\omega c}\sum_{L=l_i\pm1}|\langle Lk^{(-)}l_in_i\|\mathcal{D}\|2\ ^{1,3}S\rangle|^2. \tag{15}$$

Here $c\simeq137$ is the speed of light in atomic units and E_0 is the energy of the initial metastable state. We separate the contribution from the final channels $\langle \boldsymbol{k}^{(-)}i|$ into single and double ionization according to the energy of the ϵ_i which is positive for the double-ionized channels and negative for the singly ionized channels. We also ensure that for the negative-energy state cross sections, contributions to the ionization plus excitation cross sections are multiplied by the projection of the state onto the true target discrete subspace as is done for electron-impact ionization [23].

B. *B* splines

The Laguerre basis is a natural choice to generate a complete set of the pseudostates for a hydrogenic target, the He^+ ion in the present case. However, this choice becomes less obvious when the target has a more complicated electronic structure. In addition, the Laguerre basis is rather rigid, with only one adjustable parameter, the exponential fall-off α, which can be varied slightly to ensure a desired energy distribution of the target pseudostates. Large variation of this parameter away from the value $\alpha=Z/2$ can compromise the quality of the lowest bound states.

Instead of using the hydrogenic-like orbitals one can generate a pseudostate basis by expanding the one-electron radial orbitals in terms of piecewise polynomials, known as basis splines or B splines [24]. We write the pseudostate wave function as

$$\Phi^N_{nlm}(\boldsymbol{r})=r^{-1}P_{nl}(r)Y_{lm}(\hat{r}),$$

$$\text{where}\quad P_{nl}(r)=\sum_{i=2}^{N-1}C_iB_{i,k}(r). \tag{16}$$

Here N is the total number of splines of order k. The atomic system of interest is placed into a spherical box of a large radius R. The radial interval $[0,R]$ is divided into segments whose end points are given by the monotonically increasing

knot sequence $\{t_i\}$, $i=1,\ldots,N+k$. The B splines on this knot sequence are defined by the recurrent relations

$$B_{i,1}(r)=\begin{cases}1, & t_i\leqslant r\leqslant t_{i+1},\\ 0, & \text{otherwise},\end{cases} \tag{17}$$

$$B_{i,k}(r)=\frac{r-t_i}{t_{i+k-1}-t_i}B_{i,k-1}(r)+\frac{t_{i+k}-r}{t_{i+k}-t_{i+1}}B_{i+1,k-1}(r). \tag{18}$$

The function $B_{i,k}(r)$ is a piecewise polynomial of degree $k-1$ inside the interval $t_i\leqslant r\leqslant t_{i+1}$, and it vanishes outside this interval. The boundary conditions are implemented by removing from the summation (16) $B_1(r)$ and $B_N(r)$ which do not vanish at $r=0$ and $r=R$, respectively. The important feature of these functions is that of all the B splines of order k defined on the knot sequence $\{t_i\}$ only k of them are nonzero on each interval $[t_j,t_{j+1}]$. This feature becomes very useful for finding the expansion coefficients in Eq. (16) by solving the variational equation $\delta S=0$ where the action S is defined by the Hamiltonian of the system, most conveniently the Hartree-Fock one [17]. This variational equation can be reduced to a symmetric generalized eigenvalue problem and solved numerically using standard mathematical procedures.

The important point here is the choice of the radial grid $\{t_i\}$. Most commonly an exponential grid is used

$$t_i=t_0\{\exp[h(i-k)]-1\}, \tag{19}$$

where $k+1<i<N$ and $t_N=R$. The B splines generated on the exponential grid have exponentially increasing positive energies. This is convenient when the perturbation theory expansions are to be summed with a minimal number of terms. However, this is not sufficient in the present case of the two-electron ionization. In order to mimic the true continuum, the pseudostates should satisfy the orthogonality condition

$$\langle\chi(\boldsymbol{k})|\Phi_j^N\rangle|_{N\to\infty}=\delta(k^2/2-\epsilon_j). \tag{20}$$

By using the exponential B splines it can only be satisfied to a very poor accuracy of about 10^{-2} whereas an equal size Laguerre basis provides the orthogonality to a typical accuracy of 10^{-5}.

Our experience shows that condition (20) is much better satisfied with the splines generated on a semilogarithmic grid

$$\alpha t_i+\beta\ln t_i=t_0+(i-k)h. \tag{21}$$

The pseudostates built from the semi-logarithmic splines form an almost equidistant positive energy spectrum and satisfy the orthogonality condition to required accuracy. By adjusting the box size R and, to a lesser extent, other radial grid parameters α, β, and t_0, the density of the positive energy pseudostates can be varied. We should stress that in all cases the lowest negative energy bound states generated from the splines are the true eigenstates of the target Hamiltonian. Only when the radial extent of an orbital becomes larger than the size of the box R does it differ from the exact eigenstate.

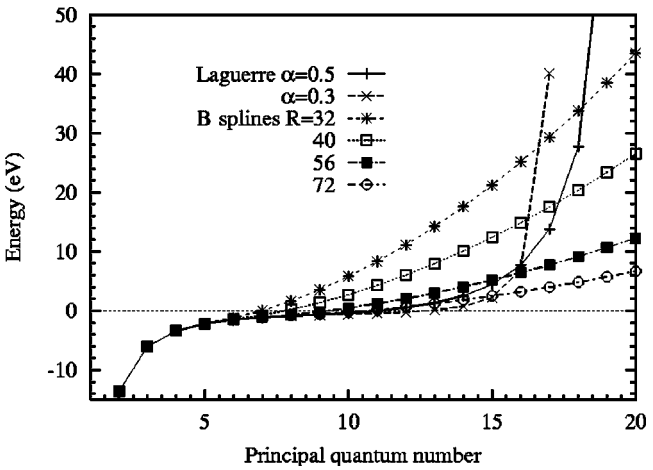

FIG. 1. Pseudostate spectra generated with different adjustable parameters: the Laguerre basis with the exponential fall-off parameter $\alpha=0.5$ and 0.3, and the B-spline basis with the radial box sizes $R=32$, 40, 56, and 72 a.u. The energies of the pseudostates are shown as dots. Continuous lines help to guide the eye.

In our calculations we used $N=75$ B splines of $k=7$ order of which 20 lowest pseudostates were included into the close-coupling expansion for each orbital momentum. The pseudostate spectra obtained with various size of the radial box R are plotted in Fig. 1 together with a comparable Laguerre state spectrum.

IV. RESULTS

A. Metastable $2\,^1S$ singlet state

In Fig. 2 we present the results of the CCC calculations of the single and double photoionization from the metastable $2\,^1S$ state from near threshold to 50 eV excess energy (60 to 110 eV photon energy). In the close-coupling expansion 85 target states with maximum orbital angular momentum $l_{\max}=4$ and $N_l=17$ were used. The exponential fall-off parameter of the Laguerre basis was set to $\alpha=0.3$ to have a more dense spectrum of pseudostates near the threshold. The number of k-grid points in the integration over the intermediate states in Eq. (14) was 64. The MCHF expansion with 14 terms was used for the initial $2\,^1S$ state. The quality of this state can be judged by the close convergence between the calculations performed in the three L, V, and A gauges. The total cross section (top panel of Fig. 2) is practically identical in the three gauges. The ratio of the double-to-single-photoionization cross sections (bottom panel) differ slightly in the three gauges but this difference does not exceed 10% on the given energy range.

The CCC results are compared with the R-matrix calculation of van der Hart *et al.* [11]. The total cross section agrees very well between the two calculations. The double-to-single ratio is slightly higher in the CCC theory. This difference increases away from the threshold. There is almost no oscillatory structure in the CCC results though no averaging over the photon energy was performed. The pseudoresonances, typically associated with L^2 expansions, have been elimi-

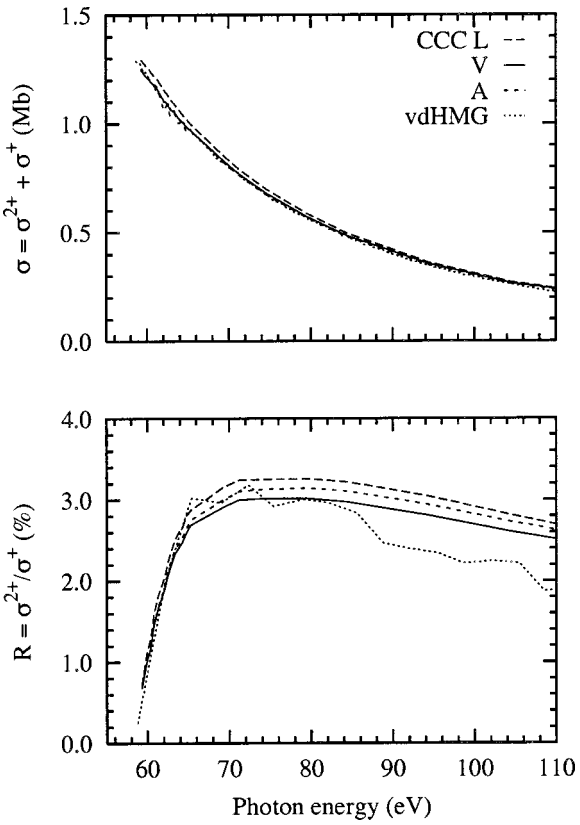

FIG. 2. The total photoionization cross section $\sigma = \sigma^{2+} + \sigma^{+}$ (top panel) and the ratio of the double-to-single-photoionization cross sections $R = \sigma^{2+}/\sigma^{+}$ (bottom panel) for the metastable $2\,^1S$ singlet state of helium. The CCC calculations in the three gauges (length, velocity and acceleration) are shown. Comparison is made with the calculation of van der Hart *et al.* [11] labeled as vdHMG.

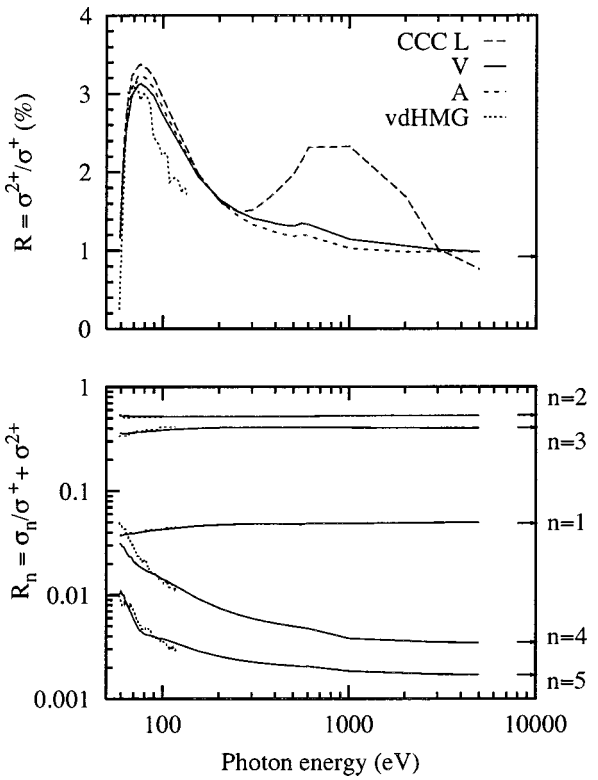

FIG. 3. The double-photoionization ratio R (top panel) and the photoionization with excitation ratios R_n (bottom panel) of the helium $2\,^1S$ state. Same notations are used as in Fig. 2. The asymptotic limits of the infinite photon energy (see Table I) are indicated by the arrows.

nated by choosing a sufficiently large size of the pseudostate basis.

The same double-to-single cross-section ratio is presented in Fig. 3 over an extended photon energy range. Here also shown are the partial EPI ratios $R_n = \sigma_n/(\sigma^{+} + \sigma^{++})$. These results are a combination of several CCC calculations. We set $\alpha = 0.3$ for the near-threshold calculation. Increased it to $\alpha = 0.5$ in the intermediate region below 1 keV and further increased it to $\alpha = 1.0$ at very large photon energies up to 10 keV. For the DPI calculation the length form becomes unreliable at the photon energy of several hundred eV. The other two forms, velocity and acceleration, keep close together and gradually approach the asymptotic limit of infinite photon energy $R^{\infty} = 0.92\%$ (see Table I). The same behavior was observed for the CCC calculation on the helium ground state [13]. The three gauge CCC calculations for the partial EPI ratios R_n remain indistinguishable at all photon energies (only the V form is shown in the figure). These ratios also gradually approach the asymptotic values shown in Table I. As in Fig. 2 comparison is made with the R-matrix calculation of van der Hart *et al.* [11] available on a limited photon energy range. Where available, their ratios R_n agree well with the CCC results except for the $n = 4$ ratio which is slightly higher for low photon energies.

In Fig. 4 we investigate the near-threshold behavior of the DPI cross section. The CCC calculation for the helium ground state [13] clearly indicated the Wannier regime $\sigma^{2+} \propto E^{1.056}$ at the excess energy E below 1 eV. In the case of the $2\,^1S$ metastable helium state this behavior is not so easily detected from the CCC calculation. The near-threshold CCC calculations are very difficult as both required $l_{\max}$ and N_l increase [25]. Limited computational resources presently do not allow for accurate CCC results below 1 eV excess en-

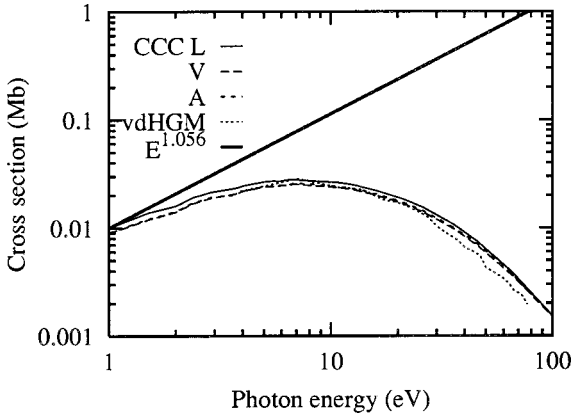

FIG. 4. The double-photoionization cross section near the threshold. Same notation as in Fig. 2 is used. The Wannier asymptote $E^{1.056}$ is drawn to the best visual fit of the data and is indicated by a thick straight line.

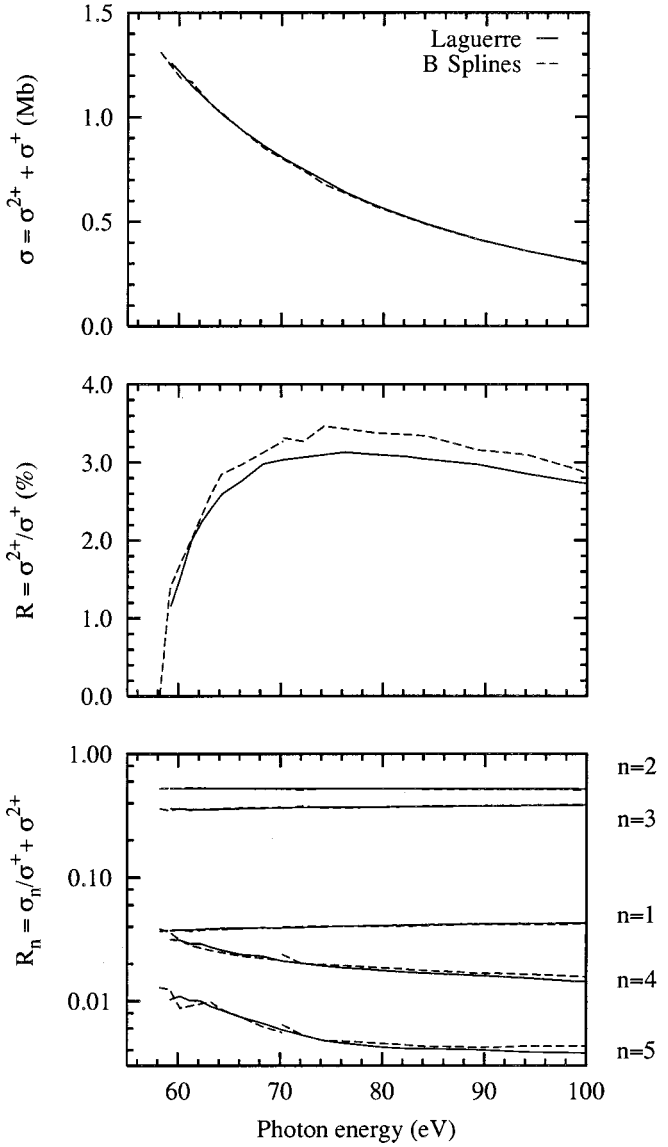

FIG. 5. The total-photoionization cross section (top panel), the DPI ratio R (middle panel), and the EPI ratios R_n (bottom panel) for the $2\,^1S$ state of helium. Close-coupling calculations with the Laguerre basis and B splines in the V form are shown by the solid and dashed lines, respectively.

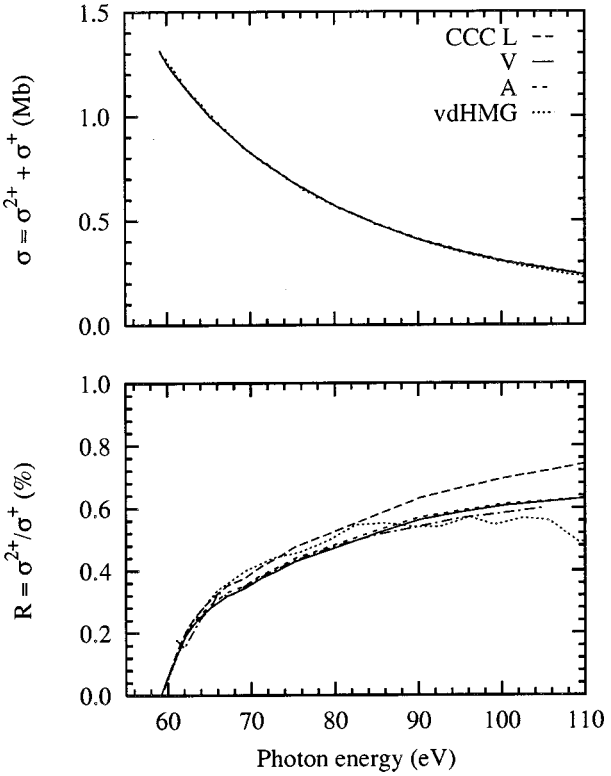

FIG. 6. The total-photoionization cross section $\sigma = \sigma^{2+} + \sigma^{+}$ (top panel) and the ratio of the double-to-single-photoionization cross sections $R = \sigma^{2+}/\sigma^{+}$ (bottom panel) for the $2\,^3S$ state of helium. The CCC calculations in the three gauges (length, velocity, and acceleration) are shown. Comparison is made with the calculation of van der Hart *et al.* [11] labeled as vdHMG.

ergy. It may be that the Wannier regime for this metastable state starts even closer, if at all, to the threshold than in the case of DPI from the ground-state helium.

The results of the close-coupling calculation with B splines are shown in Fig. 5 and compared with the CCC calculations. Only the V-form close-coupling calculations are shown for clarity. The gauge difference for the B-spline calculations is of the same order (less than 10%) as for the CCC calculations. The B-spline calculation was performed with $l_{\max}=4$ and $N_l=20$. To avoid the pseudoresonance oscillations in the DPI cross section a careful choice of the basis had to be made. The near-threshold region (below 70 eV photon energy) was calculated with a very fine semilogarithmic grid generated with the size of the spherical box $R=72$ a.u. As is seen form Fig. 1 the spectrum of positive energy pseudostates in this case is very dense and narrow. The first 20 states have only a 6 eV span. Further away from threshold, at photon energies above 70 eV another set of pseudostates was used calculated with $R=56$ a.u. The B-spline DPI calculation differs only slightly from the accurate CCC result. The EPI results, both for the CCC and B-spline calculations are very close to each other.

B. Metastable $2\,^3S$ triplet state

Results of the CCC calculations of the DPI and EPI from the helium $2\,^3S$ state are presented in Figs. 6–8. The total and double photoionization cross-sections are shown in Fig. 6 together with the corresponding data of van der Hart *et al.* [11]. As in the case of the singlet state, the CCC calculation starts to deviate from the R-matrix results at the higher photon energies. This tendency is clearly visible in Fig. 7 where the DPI and EPI ratios are shown over the extended photon energy range. As in the case of the singlet state the CCC L-form calculation quickly loses its accuracy but the two other forms V and A remain very close together up to several keV. Here the DPI and EPI ratios almost reach their asymptotic limits shown in Table I. The CCC-calculated EPI ratios agree with the predictions of the R-matrix theory (where available) except for a slight deviation in the case of $n=4$. The DPI cross section in the near-threshold region is shown in Fig. 8. The Wannier regime appears to be ap-

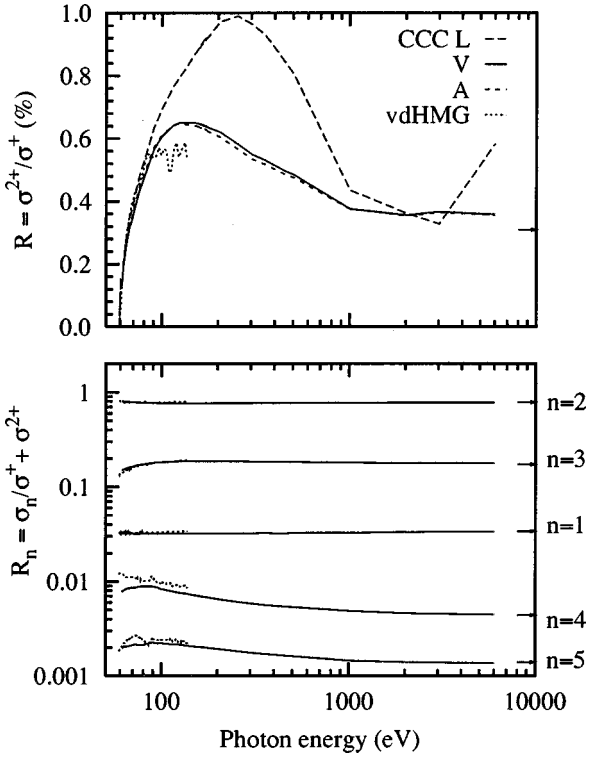

FIG. 7. The DPI ratio R (top panel) and the EPI ratios R_n (bottom panel) for the metastable $2\,^3S$ state of helium. Same notation as in Fig. 6 is used. The asymptotic limits of the infinite photon energy (see Table I) are indicated by the arrows.

proached by the CCC and R-matrix calculations. However, calculations at even lower energies are necessary to confirm this.

V. TWO-ELECTRON PHOTOIONIZATION AND ELECTRON-IMPACT IONIZATION

Samson and collaborators [26,27] have noticed a remarkable similarity in the shape of the DPI ratio R, plotted as a function of the excess energy above the DPI threshold, and the cross section of the electron impact ionization (EII) of the corresponding singly charged ion. They expressed this as a proportionality relation

$$\frac{\sigma^{2+}(E)}{\sigma^{+}(E)} = \frac{\sigma_e^{+}(E)}{a\pi r^2}, \tag{22}$$

where r is the radius of the electron-ion interaction zone and a is a dimensionless constant of the order of 1. This proportionality was found in several atomic targets (He, Ne, and O) on a wide range of excess energies E above threshold. This was interpreted by Samson and coworkers as the dominance of the two-stage mechanism of the two-electron photoionization in which the first stage of the single photoionization was followed by the EII of the singly charged ion.

As our theoretical model is built explicitly on the assumption of this two-stage mechanism, we should observe the proportionality (22) in our calculations as well. Because the

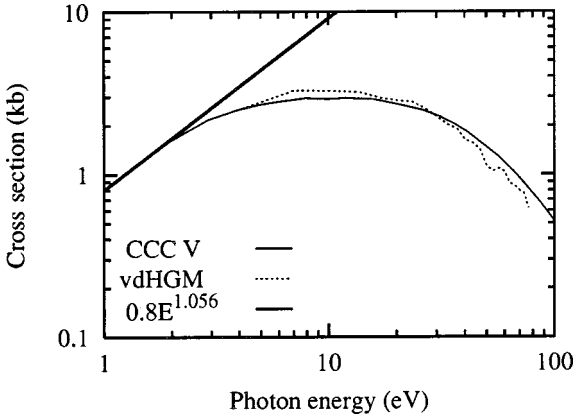

FIG. 8. The low-energy double-photoionization cross section. Same notation as in Fig. 6 is used.

calculated cross sections are not affected by experimental uncertainties the desired relation would be much easier to establish. The only essential difference with the model of Samson *et al.* [26,27] is that in our formalism the EII takes place with the total orbital angular momentum of the electron-ion system $J=1$ and the same total spin as that of the initial state of helium S_0. Whereas Samson *et al.* [26,27] considered the total EII cross section summed over all J from 0 to infinity and both spins.

In Fig. 9 we plot the DPI ratio and the cross-section of the EII of the He^+ ion (only for $J=1$, $S=S_0$). The three initial helium states are considered: the ground $1\,^1S$ and the two metastable states $2\,^{1,3}S$. In the case of the ground state the most dominant channel of the single photoionization is to the He^+ ground state. Accordingly we scale the DPI ratio R with the EII cross section of the He^+ ground state. For the metastable states the most probable outcome of the single photoionization is formation of the $2s$ He^+ state. In this case we scale the DPI ratio with the EII cross section of He^+ in the $2s$ excited state, of the singlet and triplet channels, respectively, for the $2\,^1S$ and $2\,^3S$ states. We note that the DPI ratio and the EII cross section are extracted from the same CCC calculation.

The proportionality (22) is indeed seen from Fig. 9, at least near the threshold. It is best satisfied for the ground state in an excess energy range of about 20 eV. It is much narrower than the 200 eV proportionality range established by Samson [26]. The primary reason for the difference is due to the absence of the higher partial waves in forming the EII cross sections. In the case of the metastable singlet and triplet states relation (22) is only satisfied for the first 10 and 5 eV above the threshold, respectively. The scaling coefficients are substantially different in the case of the ground and metastable states helium atom. For the ground state He the electron-ion interaction radius $r=0.70$ a.u. which is comparable with the size of the $1s$ orbital in the He^+ ion. For the metastable singlet state $r=1.32$ a.u. which again is comparable with the size of the $2s$ orbital of the He^+ ion.

The case of the triplet metastable state is quite different. Not only does the proportionality region shrinks to nearly 5 eV, but the size of the electron-ion interaction region becomes very large: $R=6.26$ a.u. A plausible explanation for

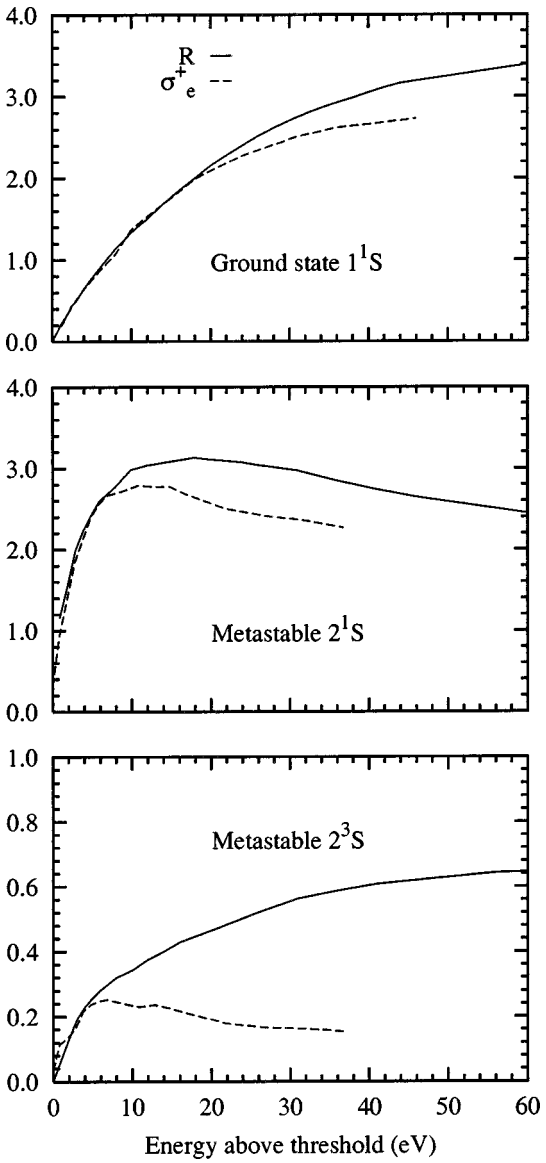

FIG. 9. The DPI ratio R (in %) and the electron impact ionization cross-section of the He^+ ion σ_e^+, scaled to match R near threshold, as a function of the excess energy.

this phenomenon is that the Pauli exclusion principle keeps the two electrons far apart.

Departure from the proportionality relation (22) is easy to understand. Simultaneously with the two-stage double photoionization there is a competing shake-off process in which the doubly ionized state is formed through the rearrangement of the ionic core after one atomic electron is removed. It is this shake-off mechanism which becomes dominant at large photon energies and leads to the asymptotic DPI and EPI ratios (3). The shake-off mechanism does not involve the EII of the ion and therefore does not satisfy the proportionality relation (22). Gradual departure from this relation means shifting the balance from the two-stage mechanism towards the shake-off mechanism as the excess energy grows.

It is well known that near the DPI threshold the two photoelectrons leave the atom with approximately equal energies and therefore their interaction is strong. This favors the two-stage mechanism. As the excess energy grows the energy sharing becomes more asymmetric with one fast and one slow photoelectrons leaving the atom. In this case the inter-electron interaction becomes weaker and the relative contribution of the two-stage mechanism diminishes as compared with the shake-off mechanism. Shifting the balance from the two-stage mechanism to the shake-off would take place sooner for the metastable $2\,^{1,3}S$ states in which the $1s$ and $2s$ electrons are better separated than in the $1s^2$ electrons in the ground state. In the triplet state the electron separation is even stronger because of the Pauli exclusion principle. This may explain the behavior observed in Fig. 9.

VI. CONCLUSION

We investigated the two-electron photoionization processes, the DPI and EPI, from the metastable helium singlet and triplet states. Close-coupling calculations were performed with a large Laguerre basis (the CCC model) and a *B*-spline basis. The CCC calculation covers a wide photon energy range from the threshold to few keV where our results reach the shake-off limit. The CCC total cross sections were generally found to be in good agreement with the *R*-matrix calculation of van der Hart *et al.* [11]. The DPI and EPI ratios are also consistent with a small disagreement in the DPI ratios away from the threshold. Near the DPI threshold there is some indication of the Wannier regime.

The *B*-spline calculation of the DPI is the first of its kind. It is demonstrated that, despite of placing the scattering system in a box of a finite size, a smooth DPI ratio can be obtained without severe pseudoresonance oscillations. The *B*-spline results are consistent with those obtained from the CCC theory.

The proportionality of the DPI cross-sections ratio and the EII cross section was investigated for the helium atom ground state and the two $2\,^{1,3}S$ metastable states. These three states form a sequence in which the relative contribution of the shake-off mechanism is gradually increasing over the contribution of the two-stage mechanism. This leads to the departure from the proportionality between the DPI ratio and EII cross section. We hope that the present work will stimulate experimental studies of the two-electron photoionization from the metastable helium.

ACKNOWLEDGMENTS

One of the authors (A.N.I.) wishes to thank the Research School of Physical Science and Engineering at the Australian National University for hospitality and financial support. Support of the Australian Research Council and the South Australian Center for High Performance Computing and Communications is gratefully acknowledged.

[1] J. S. Briggs and V. Schmidt, J. Phys. B **33**, R1 (2000).
[2] R. Stebbings, F. B. Dunning, F. K. Tittel, and R. D. Rundel, Phys. Rev. Lett. **30**, 815 (1973).
[3] M. D. Hoogerland *et al.*, Aust. J. Phys. **49**, 567 (1996).
[4] D. W. Norcross, J. Phys. B **4**, 652 (1971).
[5] V. Jacobs and P. Burke, J. Phys. B **5**, 2272 (1972).
[6] V. Jacobs, Phys. Rev. A **9**, 1938 (1973).
[7] B. Zhou and C. D. Lin, Phys. Rev. A **49**, 1057 (1994).
[8] T. N. Chang and M. Zhen, Phys. Rev. A **47**, 4849 (1993).
[9] Z. Teng and R. Shakeshaft, Phys. Rev. A **49**, 3597 (1994).
[10] R. C. Forrey *et al.*, Phys. Rev. A **51**, 2112 (1995).
[11] H. W. van der Hart, K. W. Meyer, and C. H. Greene, Phys. Rev. A **57**, 3641 (1998).
[12] A. S. Kheifets and I. Bray, Phys. Rev. A **54**, R995 (1996).
[13] A. S. Kheifets and I. Bray, Phys. Rev. A **57**, 2590 (1998).
[14] A. S. Kheifets and I. Bray, Phys. Rev. A **58**, 4501 (1998).
[15] A. S. Kheifets and I. Bray, J. Phys. B **31**, L447 (1998).
[16] A. S. Kheifets and I. Bray, Phys. Rev. Lett. **81**, 4588 (1998).
[17] J. Sapirstein and W. R. Johnson, J. Phys. B **29**, 5213 (1996).
[18] K. G. Dyall *et al.*, Comput. Phys. Commun. **55**, 425 (1989).
[19] A. Dalgarno and A. L. Stewart, Proc. R. Soc. London **76**, 49 (1960).
[20] I. Bray, Phys. Rev. A **49**, 1066 (1994).
[21] M. Y. Amusia, in *Atomic Photoeffect*, edited by K. T. Taylor (Plenum Press, New York, 1990).
[22] I. Bray and A. T. Stelbovics, Adv. At. Mol. Phys. **35**, 209 (1995).
[23] I. Bray and A. T. Stelbovics, Phys. Rev. Lett. **70**, 746 (1993).
[24] C. de Boor, *A Practical Guide to Splines* (Springer, New York, 1978).
[25] A. S. Kheifets and I. Bray, Phys. Rev. A (to be published).
[26] J. A. R. Samson, Phys. Rev. Lett. **65**, 2861 (1990).
[27] J. A. R. Samson, R. J. Bartlett, and Z. X. He, Phys. Rev. A **46**, 7277 (1992).